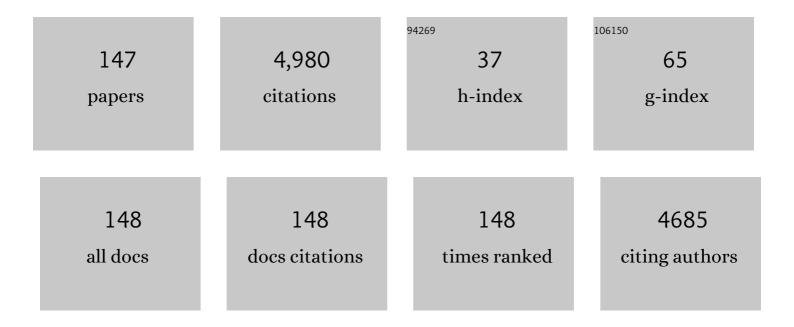
Thomas H Mareci

List of Publications by Year in descending order

Source: https://exaly.com/author-pdf/9431475/publications.pdf Version: 2024-02-01



#	Article	IF	CITATIONS
1	Acrossâ€vendor standardization of semi‣ASER for singleâ€voxel MRS at 3T. NMR in Biomedicine, 2021, 34, e4218.	1.6	43
2	Restoration of breathing after opioid overdose and spinal cord injury using temporal interference stimulation. Communications Biology, 2021, 4, 107.	2.0	21
3	Deuterated water imaging of the rat brain following metabolism of [² H ₇]glucose. Magnetic Resonance in Medicine, 2021, 85, 3049-3059.	1.9	16
4	Evaluation of early microstructural changes in the R6/1 mouse model of Huntington's disease by ultra-high field diffusion MR imaging. Neurobiology of Aging, 2021, 102, 32-49.	1.5	15
5	Functional connectivity of key resting state networks and objectively measured physical activity in older adults with joint pain: A pilot study. Experimental Gerontology, 2021, 153, 111470.	1.2	2
6	Assessing neuraxial microstructural changes in a transgenic mouse model of early stage Amyotrophic Lateral Sclerosis by ultraâ€high field MRI and diffusion tensor metrics. Animal Models and Experimental Medicine, 2020, 3, 117-129.	1.3	4
7	An MRI-based switched gradient impulse response characterization method with uniform eigenmode excitation. Journal of Magnetic Resonance, 2020, 313, 106720.	1.2	0
8	MRI of Whole Rat Brain Perivascular Network Reveals Role for Ventricles in Brain Waste Clearance. Scientific Reports, 2019, 9, 11480.	1.6	21
9	Better Brain and Cognition Prior to Surgery Is Associated With Elevated Postoperative Brain Extracellular Free-Water in Older Adults. Frontiers in Aging Neuroscience, 2019, 11, 117.	1.7	8
10	Unveiling early cortical and subcortical neuronal degeneration in ALS mice by ultra-high field diffusion MRI. Amyotrophic Lateral Sclerosis and Frontotemporal Degeneration, 2019, 20, 549-561.	1.1	25
11	Detection of axonal degeneration in a mouse model of Huntington's disease: comparison between diffusion tensor imaging and anomalous diffusion metrics. Magnetic Resonance Materials in Physics, Biology, and Medicine, 2019, 32, 461-471.	1.1	28
12	Phase contrast MRI of creeping flows using stimulated echo. Journal of Magnetic Resonance, 2019, 299, 49-58.	1.2	12
13	Longitudinal evaluation of tumor microenvironment in rat focal brainstem glioma using diffusion and perfusion MRI. Journal of Magnetic Resonance Imaging, 2019, 49, 1322-1332.	1.9	2
14	Low-Frequency Conductivity Tensor Imaging of the Human Head <italic>In Vivo</italic> Using DT-MREIT: First Study. IEEE Transactions on Medical Imaging, 2018, 37, 966-976.	5.4	43
15	Methods to Compare Predicted and Observed Phosphene Experience in tACS Subjects. Neural Plasticity, 2018, 1-10.	1.0	11
16	Temporal lobe epilepsy affects spatial organization of entorhinal cortex connectivity. Epilepsy and Behavior, 2018, 88, 87-95.	0.9	6
17	Cognition and connectomes in nondementia idiopathic Parkinson's disease. Network Neuroscience, 2018, 2, 106-124.	1.4	12
18	Editorial: Novel Tools for the Study of Structural and Functional Networks in the Brain. Frontiers in Physics, 2018, 6, .	1.0	0

#	Article	IF	CITATIONS
19	Ultra-High Field Diffusion MRI Reveals Early Axonal Pathology in Spinal Cord of ALS mice. Translational Neurodegeneration, 2018, 7, 20.	3.6	21
20	Neurite orientation dispersion and density imaging can detect presymptomatic axonal degeneration in the spinal cord of ALS mice. Functional Neurology, 2018, 33, 155-163.	1.3	18
21	Imaging of current flow in the human head during transcranial electrical therapy. Brain Stimulation, 2017, 10, 764-772.	0.7	42
22	Metal Transporter <i>Zip14</i> (<i>Slc39a14</i>) Deletion in Mice Increases Manganese Deposition and Produces Neurotoxic Signatures and Diminished Motor Activity. Journal of Neuroscience, 2017, 37, 5996-6006.	1.7	87
23	The hippocampus: detailed assessment of normative two-dimensional measurements, signal intensity, and subfield conspicuity on routine 3T T2-weighted sequences. Surgical and Radiologic Anatomy, 2017, 39, 1149-1159.	0.6	8
24	Comparisons between in-vivo current density images and computational models in human TACS recipients. Brain Stimulation, 2017, 10, e30-e31.	0.7	0
25	Small Worldness in Dense and Weighted Connectomes. Frontiers in Physics, 2016, 4, .	1.0	10
26	Toward 20ÂT magnetic resonance for human brain studies: opportunities for discovery and neuroscience rationale. Magnetic Resonance Materials in Physics, Biology, and Medicine, 2016, 29, 617-639.	1.1	66
27	A fractal derivative model for the characterization of anomalous diffusion in magnetic resonance imaging. Communications in Nonlinear Science and Numerical Simulation, 2016, 39, 529-537.	1.7	93
28	Voxelized Model of Brain Infusion That Accounts for Small Feature Fissures: Comparison With Magnetic Resonance Tracer Studies. Journal of Biomechanical Engineering, 2016, 138, 051007.	0.6	15
29	A majority rule approach for region-of-interest-guided streamline fiber tractography. Brain Imaging and Behavior, 2016, 10, 1137-1147.	1.1	20
30	Test-retest reliability of high angular resolution diffusion imaging acquisition within medial temporal lobe connections assessed via tract based spatial statistics, probabilistic tractography and a novel graph theory metric. Brain Imaging and Behavior, 2016, 10, 533-547.	1.1	13
31	Gray and White Matter Contributions to Cognitive Frontostriatal Deficits in Non-Demented Parkinson's Disease. PLoS ONE, 2016, 11, e0147332.	1.1	31
32	Characterizing magnetic resonance signal decay due to gaussian diffusion: The path integral approach and a convenient computational method. Concepts in Magnetic Resonance Part A: Bridging Education and Research, 2015, 44, 203-213.	0.2	8
33	Temporal Lobe and Frontal-Subcortical Dissociations in Non-Demented Parkinson's Disease with Verbal Memory Impairment. PLoS ONE, 2015, 10, e0133792.	1.1	20
34	Broca's area – Thalamic connectivity. Brain and Language, 2015, 141, 80-88.	0.8	45
35	High-field magnetic resonance imaging of the human temporal lobe. NeuroImage: Clinical, 2015, 9, 58-68.	1.4	19
36	Dimensionless, Scale Invariant, Edge Weight Metric for the Study of Complex Structural Networks. PLoS ONE, 2015, 10, e0131493.	1.1	14

#	Article	IF	CITATIONS
37	Classification of Fractional Order Biomarkers for Anomalous Diffusion Using q-Space Entropy. Critical Reviews in Biomedical Engineering, 2014, 42, 63-83.	0.5	3
38	On random walks and entropy in diffusionâ€weighted magnetic resonance imaging studies of neural tissue. Magnetic Resonance in Medicine, 2014, 71, 617-627.	1.9	97
39	Fractional order measures of anomalous diffusion in healthy aging of neural tissue. , 2014, , .		0
40	Absolute magnetic susceptibility of rat brain tissue. Magnetic Resonance in Medicine, 2014, 72, 876-879.	1.9	5
41	On random walks and entropy in diffusion-weighted magnetic resonance imaging studies of neural tissue. Magnetic Resonance in Medicine, 2014, 71, spcone-spcone.	1.9	1
42	Generalized Framework to Study Brain Weighted Networks. Biophysical Journal, 2013, 104, 164a.	0.2	0
43	MR measurement of alloy magnetic susceptibility: Towards developing tissue-susceptibility matched metals. Journal of Magnetic Resonance, 2013, 233, 49-55.	1.2	10
44	Characterization of anomalous diffusion in porous biological tissues using fractional order derivatives and entropy. Microporous and Mesoporous Materials, 2013, 178, 39-43.	2.2	136
45	Phase shift in the 24-hour rhythm of hippocampal EEG spiking activity in a rat model of temporal lobe epilepsy. Journal of Neurophysiology, 2013, 110, 1070-1086.	0.9	11
46	Segmentation of Rat Brain MR Images Using Artificial Neural Network Classifier. , 2013, , .		0
47	Broca's area and its striatal and thalamic connections: a diffusion-MRI tractography study. Frontiers in Neuroanatomy, 2013, 7, 8.	0.9	88
48	Imaging White Matter in Human Brainstem. Frontiers in Human Neuroscience, 2013, 7, 400.	1.0	36
49	Influence of Neuropathology on Convection-Enhanced Delivery in the Rat Hippocampus. PLoS ONE, 2013, 8, e80606.	1.1	3
50	Voxelized Computational Model for Convection-Enhanced Delivery in the Rat Ventral Hippocampus: Comparison with In Vivo MR Experimental Studies. Annals of Biomedical Engineering, 2012, 40, 2043-2058.	1.3	26
51	Magnetic resonance imaging and volumetric analysis: Novel tools to study the effects of thyroid hormone disruption on white matter development. NeuroToxicology, 2012, 33, 1322-1329.	1.4	21
52	Role of convection and diffusion on DCE-MRI parameters in low leakiness KHT sarcomas. Microvascular Research, 2012, 84, 306-313.	1.1	16
53	Dynamic contrast-enhanced MRI of Gd-albumin delivery to the rat hippocampus in vivo by convection-enhanced delivery. Journal of Neuroscience Methods, 2012, 209, 62-73.	1.3	13
54	Nuclear magnetic resonance energy harvesting for ultra-low power biomedical implants. , 2011, , .		2

Nuclear magnetic resonance energy harvesting for ultra-low power biomedical implants. , 2011, , . 54

#	Article	IF	CITATIONS
55	Sensitivity Analysis of an Image-Based Solid Tumor Computational Model with Heterogeneous Vasculature and Porosity. Annals of Biomedical Engineering, 2011, 39, 2360-2373.	1.3	84
56	In Vivo Contrast-Enhanced MR Imaging of Direct Infusion into Rat Peripheral Nerves. Annals of Biomedical Engineering, 2011, 39, 2823-2834.	1.3	10
57	Phase shift in hippocampal circadian rhythm during the latent period of epileptic rats. BMC Neuroscience, 2011, 12, .	0.8	1
58	Voxelized 3D Computational Transport Model of Infusions Into the Ventral Hippocampus: Comparison With Experimental Studies. , 2011, , .		0
59	A voxelized model of direct infusion into the corpus callosum and hippocampus of the rat brain: model development and parameter analysis. Medical and Biological Engineering and Computing, 2010, 48, 203-214.	1.6	20
60	Development of an inductively coupled MR coil system for imaging and spectroscopic analysis of an implantable bioartificial construct at 11.1 T. Magnetic Resonance in Medicine, 2010, 63, 998-1006.	1.9	12
61	Regional convection-enhanced delivery of gadolinium-labeled albumin in the rat hippocampus in vivo. Journal of Neuroscience Methods, 2010, 187, 129-137.	1.3	23
62	Granger causality relationships between local field potentials in an animal model of temporal lobe epilepsy. Journal of Neuroscience Methods, 2010, 189, 121-129.	1.3	42
63	Early MR diffusion and relaxation changes in the parahippocampal gyrus precede the onset of spontaneous seizures in an animal model of chronic limbic epilepsy. Experimental Neurology, 2010, 224, 258-270.	2.0	52
64	A Computational Model of Interstitial Transport in Murine Sarcoma With Heterogeneous Vasculature: A Sensitivity Analysis. , 2009, , .		0
65	A Physical basis for multi-fiber reconstruction from DW-MRI data. , 2009, , .		0
66	Voxelized Model of Interstitial Transport in the Rat Spinal Cord Following Direct Infusion Into White Matter. Journal of Biomechanical Engineering, 2009, 131, 071007.	0.6	17
67	In Vivo MRI of Macromolecular Transport Into the Rat Spinal Cord via Peripheral Nerve Infusion. , 2009, , .		0
68	Temporal Lobe Epilepsy: Anatomical and Effective Connectivity. IEEE Transactions on Neural Systems and Rehabilitation Engineering, 2009, 17, 214-223.	2.7	24
69	Characterization of an anisotropic hydrogel tissue substrate for infusion testing. Journal of Applied Polymer Science, 2009, 114, 1992-2002.	1.3	16
70	Circadian control of neural excitability in an animal model of temporal lobe epilepsy. Neuroscience Letters, 2009, 455, 145-149.	1.0	32
71	Postmortem interval alters the water relaxation and diffusion properties of rat nervous tissue — Implications for MRI studies of human autopsy samples. NeuroImage, 2009, 44, 820-826.	2.1	104
72	Multi-fiber Reconstruction from DW-MRI Using a Continuous Mixture of Hyperspherical von Mises-Fisher Distributions. Lecture Notes in Computer Science, 2009, 21, 139-150.	1.0	9

#	Article	IF	CITATIONS
73	Non-rigid Registration of High Angular Resolution Diffusion Images Represented by Gaussian Mixture Fields. Lecture Notes in Computer Science, 2009, 5761, 190-197.	1.0	18
74	Variational denoising of diffusion weighted MRI. Inverse Problems and Imaging, 2009, 3, 625-648.	0.6	21
75	A Computational Model of Direct Infusion Into the Rat Brain: Corpus Callosum and Hippocampus. , 2009, , .		0
76	Quantitative assessment of macromolecular concentration during direct infusion into an agarose hydrogel phantom using contrast-enhanced MRI. Magnetic Resonance Imaging, 2008, 26, 1433-1441.	1.0	43
77	Multi-fiber reconstruction from DW-MRI using a continuous mixture of von Mises-Fisher distributions. , 2008, , .		15
78	In Vivo Contrast-Enhanced MR Imaging for Direct Infusion Into Rat Peripheral Nerve. , 2008, , .		1
79	High Resolution DCE-MRI Vascular Characterization of Murine Sarcoma and Human Renal Cell Carcinoma for Computational Modeling. , 2008, , .		0
80	A CONTINUOUS MIXTURE OF TENSORS MODEL FOR DIFFUSION-WEIGHTED MR SIGNAL RECONSTRUCTION. , 2007, 4, 772-775.		2
81	Determination of Macromolecular Concentration Following Direct Infusion into Hydrogel using Contrast-Enhanced MRI. Annual International Conference of the IEEE Engineering in Medicine and Biology Society, 2007, 2007, 2887-90.	0.5	0
82	Voxelized Model of Interstitial Transport in Nervous Tissue Following Direct Infusion into White Matter. Annual International Conference of the IEEE Engineering in Medicine and Biology Society, 2007, 2007, 2114-7.	0.5	0
83	A novel tensor distribution model for the diffusion-weighted MR signal. NeuroImage, 2007, 37, 164-176.	2.1	204
84	Diffusion Basis Functions Decomposition for Estimating White Matter Intravoxel Fiber Geometry. IEEE Transactions on Medical Imaging, 2007, 26, 1091-1102.	5.4	101
85	Computational Model of Interstitial Transport in the Rat Brain Using Diffusion Tensor Imaging. , 2007, , .		0
86	An orthotopic xenograft model of intraneural NF1 MPNST suggests a potential association between steroid hormones and tumor cell proliferation. Laboratory Investigation, 2007, 87, 1092-1102.	1.7	33
87	Resolution of complex tissue microarchitecture using the diffusion orientation transform (DOT). NeuroImage, 2006, 31, 1086-1103.	2.1	346
88	Structural insights from high-resolution diffusion tensor imaging and tractography of the isolated rat hippocampus. NeuroImage, 2006, 32, 1499-1509.	2.1	69
89	Higher Rank Tensors in Diffusion MRI. Mathematics and Visualization, 2006, , 177-187.	0.4	2
90	Evolving into epilepsy: Multiscale electrophysiological analysis and imaging in an animal model. Experimental Neurology, 2006, 198, 31-47.	2.0	27

#	Article	IF	CITATIONS
91	Computational Model of Interstitial Transport in the Spinal Cord using Diffusion Tensor Imaging. Annals of Biomedical Engineering, 2006, 34, 1304-1321.	1.3	65
92	Von Mises-Fisher Mixture Model of the Diffusion ODF. , 2006, 2006, 65-68.		34
93	Segmentation of High Angular Resolution Diffusion MRI Modeled as a Field of von Mises-Fisher Mixtures. Lecture Notes in Computer Science, 2006, , 463-475.	1.0	21
94	Generalized scalar measures for diffusion MRI using trace, variance, and entropy. Magnetic Resonance in Medicine, 2005, 53, 866-876.	1.9	138
95	Fast Orientation Mapping from HARDI. Lecture Notes in Computer Science, 2005, 8, 156-163.	1.0	7
96	Evaluation of the pathologic characteristics of excitotoxic spinal cord injury with MR imaging. American Journal of Neuroradiology, 2005, 26, 1612-22.	1.2	18
97	Patterns of Gene Expression Reveal a Temporally Orchestrated Wound Healing Response in the Injured Spinal Cord. Journal of Neuroscience, 2004, 24, 8562-8576.	1.7	95
98	DT-MRI denoising and neuronal fiber tracking. Medical Image Analysis, 2004, 8, 95-111.	7.0	77
99	A Constrained Variational Principle for Direct Estimation and Smoothing of the Diffusion Tensor Field From Complex DWI. IEEE Transactions on Medical Imaging, 2004, 23, 930-939.	5.4	157
100	Anatomical Connectivity in the Central Nervous System Revealed by Diffusion Tensor Magnetic Resonance Imaging (DT-MRI). Biocomputing, 2004, , 145-169.	0.2	0
101	Generalized diffusion tensor imaging and analytical relationships between diffusion tensor imaging and high angular resolution diffusion imaging. Magnetic Resonance in Medicine, 2003, 50, 955-965.	1.9	367
102	A Constrained Variational Principle for Direct Estimation and Smoothing of the Diffusion Tensor Field from DWI. Lecture Notes in Computer Science, 2003, 18, 660-671.	1.0	30
103	Progress in high field MRI at the University of Florida. Magnetic Resonance Materials in Physics, Biology, and Medicine, 2002, 13, 152-157.	1.1	24
104	Line Integral Convolution for Visualization of Fiber Tract Maps from DTI. Lecture Notes in Computer Science, 2002, , 615-622.	1.0	9
105	Visualization of neural tissue water compartments using biexponential diffusion tensor MRI. Magnetic Resonance in Medicine, 2001, 45, 580-587.	1.9	118
106	In vivo1H magnetic resonance imaging and spectroscopy of the rat spinal cord using an inductively-coupled chronically implanted RF coil. Magnetic Resonance in Medicine, 2001, 46, 1216-1222.	1.9	43
107	NMR spectroscopy of single neurons. Magnetic Resonance in Medicine, 2000, 44, 19-22.	1.9	91
108	In vivo dynamics and distribution of intracerebroventricularly administered gadodiamide, visualized by magnetic resonance imaging. Neuroscience, 1999, 90, 1115-1122.	1.1	13

#	Article	IF	CITATIONS
109	Diffusion anisotropy in excised normal rat spinal cord measured by NMR microscopy. Magnetic Resonance Imaging, 1997, 15, 441-450.	1.0	82
110	Magnetic field gradient system for nuclear magnetic resonance microimaging. Magnetic Resonance Materials in Physics, Biology, and Medicine, 1996, 4, 85-91.	1.1	4
111	A Field-Gradient Coil Using Concentric Return Paths. Journal of Magnetic Resonance Series B, 1996, 112, 124-130.	1.6	12
112	Dynamic Assessment of Intraspinal Neural Graft Survival Using Magnetic Resonance Imaging. Experimental Neurology, 1995, 136, 64-72.	2.0	13
113	Relative Efficiencies of Weighting Methods for Phase-Encoded Localized NMR. Journal of Magnetic Resonance Series B, 1994, 103, 274-277.	1.6	6
114	A comparison of an inductively coupled implanted coil with optimized surface coils forin vivo NMR imaging of the spinal cord. Magnetic Resonance in Medicine, 1993, 30, 626-633.	1.9	50
115	In vivo magnetic resonance imaging of fetal cat neural tissue transplants in the adult cat spinal cord. Journal of Neurosurgery, 1992, 76, 261-274.	0.9	37
116	Delayed grafting of fetal CNS tissue into chronic compression lesions of the adult cat spinal cord. Restorative Neurology and Neuroscience, 1991, 2, 309-325.	0.4	19
117	Volume-localized spectroscopy using selective fourier transform with windowing by variable-tip-angle excitation. Journal of Magnetic Resonance, 1991, 94, 174-179.	0.5	7
118	Essential considerations for spectral localization using indirect gradient encoding of spatial information. Journal of Magnetic Resonance, 1991, 92, 229-246.	0.5	48
119	Suppression of artifacts in multiple-echo magnetic resonance. Journal of Magnetic Resonance, 1989, 83, 11-28.	0.5	5
120	A digital phase shifter with 7.5° resolution. Journal of Magnetic Resonance, 1989, 84, 275-281.	0.5	2
121	Application of Magnetic Resonance Imaging to Visualization of Flow in Porous Media. Nuclear Technology, 1989, 84, 113-118.	0.7	23
122	Convolution spectral imaging. Journal of Magnetic Resonance, 1988, 79, 236-254.	0.5	1
123	NMR imaging and relaxation study of polymer swelling and chain dynamics. Journal of Molecular Liquids, 1988, 38, 185-206.	2.3	24
124	Experimental study of optimal selective 180° radiofrequency pulses. Journal of Magnetic Resonance, 1988, 79, 1-10.	0.5	55
125	Selective fourier transform localization. Magnetic Resonance in Medicine, 1987, 5, 417-433.	1.9	79
126	Selective inversion radiofrequency pulses by optimal control. Journal of Magnetic Resonance, 1986, 70, 310-318.	0.5	42

#	Article	IF	CITATIONS
127	Tip-angle-reduced T1 imaging. Journal of Magnetic Resonance, 1986, 67, 55-65.	0.5	7
128	Exploiting the stimulated echo in nuclear magnetic resonance imaging. II. Applications. Journal of Magnetic Resonance, 1985, 65, 298-307.	0.5	6
129	Exploiting the stimulated echo in nuclear magnetic resonance imaging. I. Method. Journal of Magnetic Resonance, 1985, 64, 177-182.	0.5	8
130	High-resolution magnetic resonance spectra from a sensitive region defined with pulsed field gradients. Journal of Magnetic Resonance, 1984, 57, 157-163.	0.5	40
131	Practical aspects of carbon-13 double quantum NMR. Journal of Magnetic Resonance, 1983, 53, 360-363.	0.5	18
132	Mapping proton-proton coupling via double-quantum coherence. Journal of Magnetic Resonance, 1983, 51, 531-535.	0.5	81
133	Observation of 13Cî—,13C couplings with enhanced sensitivity. Journal of Magnetic Resonance, 1982, 46, 180-184.	0.5	64
134	Echoes and antiechoes in coherence transfer NMR: Determining the signs of double-quantum frequencies. Journal of Magnetic Resonance, 1982, 48, 158-163.	0.5	134
135	Weak satellite signals in high-resolution NMR spectra: Separating the wheat from the chaff. Journal of Magnetic Resonance, 1981, 42, 341-345.	0.5	69
136	Nitrogen-15 satellites in proton NMR spectra observed by two-dimensional fourier transformation. Journal of Magnetic Resonance, 1981, 44, 572-576.	0.5	2
137	13C and 1H nuclear magnetic resonance spectroscopy of C-19 and 6β-methyl substituted steroids: long-range shift effects in conformational analysis. Canadian Journal of Chemistry, 1979, 57, 27-37.	0.6	10
138	Quantitative analysis of mixtures by carbon-13 nuclear magnetic resonance spectrometry. Analytical Chemistry, 1977, 49, 2130-2136.	3.2	46
139	Chemical and radiochemical stability of the adrenal-scanning agents, 66-iodomethyl-19-norcholest-5(10)-en-3β-ol and 19-iodocholest-5-en-3β-ol. Steroids, 1977, 30, 511-519.	0.8	5
140	Synthesis and purification of radioactive 6β-iodomethyl-19-norcholest-5(10)-EN-33-ol. Steroids, 1976, 28, 295-303.	0.8	10
141	Fiber tract mapping from diffusion tensor MRI. , 0, , .		51
142	Automatic fiber tractography from DTI and its validation. , 0, , .		5
143	Simultaneous smoothing and estimation of the tensor field from diffusion tensor MRI. , 0, , .		8
144	Fiber orientation mapping using generalized diffusion tensor imaging. , 0, , .		5

#	Article	IF	CITATIONS
145	Statistical analysis of a nonlinear estimator for ADC and its application to optimizing diffusion weighting factors. , 0, , .		0
146	A Nonparametric Reconstruction and its Matrix Implementation for the Diffusion Orientation Transform (DOT). , 0, , .		0
147	Effective and Anatomical Connectivity in a Rat Model of Spontaneous Limbic Seizure. , 0, , 45-59.		0